Polym. Bull. (2012) 68:239–251
DOI 10.1007/s00289-011-0627-4

ORIGINAL PAPER

The effects of vibration field on crystal structures and orientation of isotactic polypropylene injection samples

Jie Zhang · Hong Liu · Lei Zhang · Qixiong Zhou · Xueqin Gao · Kaizhi Shen

Received: 29 October 2010 / Revised: 26 July 2011 / Accepted: 3 September 2011 /
Published online: 10 September 2011

Abstract In this study, isotactic polypropylene (iPP) samples were prepared by self-made pressure vibration injection device, in which a periodical shear field was imposed on the iPP melt during the filling and packing stages. The crystal structures and orientation of samples were investigated by wide-angle X-ray diffraction and polarizing light microscopy (PLM). The β form and γ form were found in vibration injection molding samples. Compared with the static samples, the orientation of iPP chains within lamellae was observed in the transition layer (at the depth of 1.5 mm from the surface) of the vibration injection molding samples, and the orientation was found even in the core layer. The PLM observation indicates the β form exists in the transition and core region of the vibration sample. Besides, two types of β-PP could be observed simultaneously in the core region under high magnification. The bright β crystallites (β_{III}) are fan-shaped and lie perpendicularly to the flow direction. In the other hand, the ringed β crystallites (β_{IV}) almost remain their spherulite shape. Moreover, fiber crystal was observed in vibration sample, even in the core region. Some fiber crystals in the transition region reappeared in the cooling circle after the sample was held at 180 °C for 2 min. This could be explained in structure memory effect and its high thermal stability.

Keywords Vibration injection molding · Crystal structures · Orientation · β poly (propylene) (PP) · Structure memory effect

J. Zhang (✉) · H. Liu · L. Zhang · Q. Zhou · X. Gao · K. Shen
State Key Laboratory of Polymer Materials Engineering, College of Polymer Science and Engineering, Sichuan University, Chengdu 610065, People's Republic of China
e-mail: zhangjie@scu.edu.cn

Introduction

As a universal plastic, iPP is a kind of semicrystalline polymer with multicrystal structures. Different crystallization conditions and molecular characteristics can lead to four basic crystalline forms: monoclinic α-form, trigonal β-form, orthorhombic γ-form, and mesomorphic smectic form [1–4]. Among these crystalline forms, the α form is commonly detected in iPP, while the metastable β-crystal may be generated under some special conditions, such as quenching the melt to a certain temperature range [2], directional crystallization in a temperature gradient field [5], shearing or elongation of the melt during crystallization [6–8], or addition of heterogeneous nucleating agents into the sample [9–15]. The γ-crystal may be formed in degraded, low molecular weight iPP, in samples crystallized under high pressure, or under pronounced molecular orientation [2, 4, 16–18]. Different crystal structures have different effects on the properties of product. For example, the impact on strength and toughness of β-PP were found to exceed those of α-PP, which can be attributed to the peculiar lamellar morphology of β-PP [19, 20].

During polymer processing, processing conditions greatly affect the rheological behavior of polymer melt, therefore decide directly the microstructure of product and its performance. For injection molding, iPP sample is molded under the imposition of flow fields (shear, elongation, and mixed) and temperature field. Those effects together lead to skin–core structure along the depth direction in the sample [18, 21, 22]. In the past two decades, melt vibration technology in injection molding has attracted extensive interests [13, 23–28] and some valuable results have been achieved. Bevis and co-workers [29, 30] and Zhang et al. [31, 32] utilized oscillating packing injection molding (OPIM) to investigate morphology of iPP vibration sample. It is shown that the β-PP and γ-PP crystal can be induced, and the orientation of iPP samples can be changed by vibration technique. However, neither the structures and distribution of β-PP of vibration sample nor the quantitative study of the change in the degree of orientation has not been further investigated. In this article, we utilized self-made vibration injection device to mold iPP samples and investigated those unsolved problems by WAXD and PLM equipped with hot stage.

Experimental section

Apparatus

The schematic representation of the pressure vibration equipment is shown in Fig. 1. The vibration or injection ram is driven by vibration and injection system. The injection system provides the base pressure while the vibration system leads to pulsant pressure. Conventional injection molding could be realized without the movement of vibration system. In the vibration injection molding, periodically changing pressure acts on the melt in the runner and mold cavity during injection and packing stages; this brings about compression and decompression on the melt and shear effect at the melt-solid interface as solidification progresses in the mold. Three parameters, including melt temperature (T_m), vibration frequency (f), and

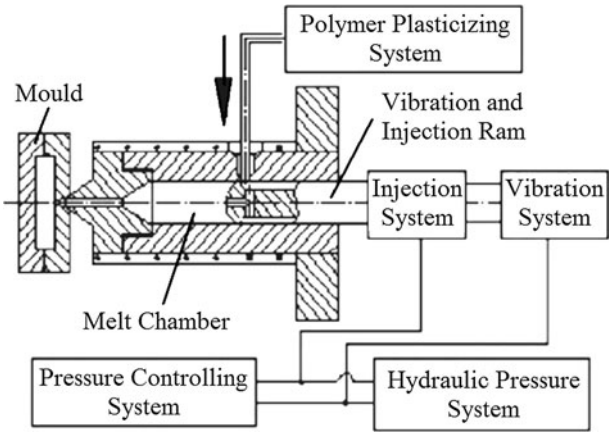

Fig. 1 The schematic representation of vibration injection molding

vibration pressure (P_v) were changed in our experiment. Vibration pressure represents the maximum value of the pulsation pressure.

Materials

The iPP (model F401) used in the experiment was a commercial product from Yan Shan Petroleum Chemical (People's Republic of China), Mw = 7.8×10^4 g mol^{-1}, MFI = 1.87 g min^{-1}.

Sample preparation

At first, iPP was melt and pumped into the melt chamber. After keeping in the set temperature for 10 min, the melt was injected into the mold cavity with or without melt vibration. The specimen obtained by vibration injection molding is called vibration sample, and the specimen obtained by static injection molding is called static sample. The processing parameters of every sample are listed in Table 1 and the bump-bell like sample is shown in Fig. 2.

Table 1 Processing parameters of samples

Processing parameters	Sample a	Sample b	Sample c
Injection pressure (MPa)	40	40	40
Packing pressure (MPa)	40	40	40
Melt temperature (°)	230	230	190
Mold temperature (°)	40	40	40
Vibration pressure (MPa)	0	75	35
Vibration frequency (Hz)	0	0.5	1.5

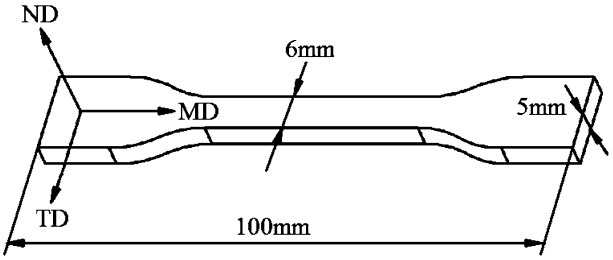

Fig. 2 The shape and dimension of the bump-bell like sample

Characterization

The one-dimensional wide-angle X-ray diffraction (1D-WAXD) measurements using a Siemens D500 diffractometer were conducted. The wavelength of the monochrome X-ray from CuKa radiation was 0.154 nm and reflection mode was used. The scanning 2θ range was from 10° to 25° with a scanning rate of 5°/min. The specimens were ground and polished at the depth of 1.5 mm below the surface which was parallel to the TD-MD plane, as shown in Fig. 3. The scan direction was the flow direction.

The two-dimensional WAXD (2D-WAXD) experiments were carried out at room temperature upon the U7B beam line in the National Synchrotron Radiation Laboratory (NSRL), University of Science and Technology of China, Hefei. The wavelength used was 0.1548 nm and the sample-to-detector distance was 220 mm. The 2D-WAXD patterns were recorded in every 180 s by a Mar CCD 165 X-ray detector system. The samples were placed with the orientation (flow direction) perpendicular to the beams, as shown in Fig. 3. All the 2D-WAXD patterns given in this study have been extracted the background thus allowed a qualitative

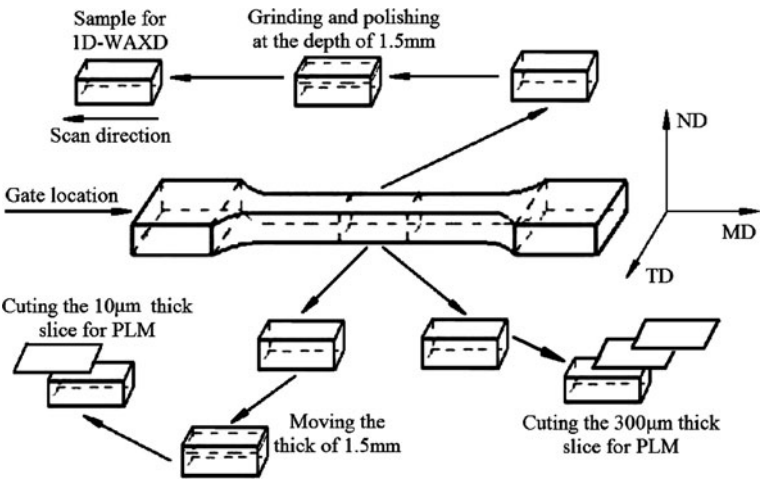

Fig. 3 Schematic drawing of sample preparation for each analysis

comparison between different samples. The Fit-2D software package was used to analyze the 2D-WAXD patterns.

Polarizing light observations were performed using a Leica DMIP PLM equipped with a Linkam THMS 600 hot stage under crossed polarizer. 10 μm thick slice was cut by microtome at the depth of 1.5 mm from the surface which was parallel to MD-TD plane, as shown in Fig. 3, and then inserted between two microscope cover glasses. Heating and cooling processes were also employed. Slice was heated from 25 to 180 °C at a heating rate of 5 °C/min, kept at 180 °C for 2 min, and then cooled to 25 °C at a cooling rate of 10 °C/min. Pictures were taken at intervals.

Results and discussion

1D-WAXD analysis

The 1D-WAXD measurements could be employed to identify crystal form of iPP. Typical diffraction peaks of the monoclinic α-crystal are at 2θ of 14.1° (110), 16.8° (040), 18.6° (130), 21.2° (111), and 21.9° (131), and those of the β-crystal are at 16° (300) and 21.2° (301). Furthermore, the diffraction peak of γ-crystal is at $2\theta = 20.1°$ for crystal plane (117) [2].

Figure 4 is the 1D-WAXD patterns of iPP injection samples prepared under the various processing parameters. For the static sample a, only the peaks representative of α-PP can be observed. But for the vibration sample b, which was obtained at $f = 0.5$ Hz, $P_v = 75$ MPa, and $T_m = 230$ °C, the peak of the (300) β-PP reflection is obvious at 2θ of 16°. This indicates that large amount of β-PP exists in the vibration sample b. Figure 4c shows the 1D-WAXD diagrams of the vibration sample c which was obtained at $f = 1.5$ Hz, $P_v = 35$ MPa, and $T_m = 190$ °C. The β-PP can also be observed. However, when compared with Fig. 4c, the intensity of β-PP of Fig. 4b decreases obviously. Furthermore, striking difference shows up in the Fig. 4c, besides α-PP and β-PP, γ-PP can be observed at 2θ of 20.1°. Another difference in Fig. 4c is that the intensity of the peak at 2θ of 16.8° (040) is prominently stronger than that of any other diffraction patterns in Fig. 4. It can be concluded that the b axis of α-PP has a pronounced orientation.

2D-WAXD analysis

Figure 5 shows 2D-WAXD patterns of static samples and vibration samples, which can evaluate orientation within crystals planes, related to the orientation of iPP chains. The flow direction is horizontal. For the static sample, the patterns of the core layer and the transition layer (at the depth of 1.5 mm from the surface) are presented full Debye rings or near-isotropic rings, as shown in Fig. 5c, e, while that of the skin layer exhibit arcing, as shown in Fig. 5a. The rings on the patterns of the core layer and the transition layer of static sample are identified from the inner to the outer ring, (110) α, (040) α, (130) α, (111) α + (041) α, (−131) α, (060) α, and (220) α. Those full Debye rings or near-isotropic rings reveal the absence of a pronounced orientation. Moreover, those patterns indicate β-form crystal does not exist in those

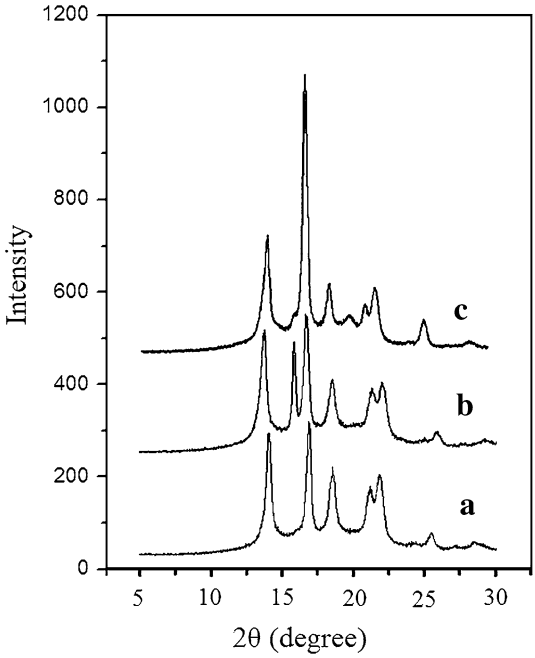

Fig. 4 1D-WAXD pattern of *a* static sample, *b* vibration sample b, and *c* vibration sample c

layers. The rings on the pattern of the skin layer of static are identified from the inner to the outer ring, (110) α, (300) β, (040) α, (130) α, (111) α + (041) α, (−131) α, (060) α, and (220) α. Almost all the Debye rings exhibit arcing, which indicate orientation in the skin layer of static sample.

For the vibration sample prepared under the processing parameters of $f = 0.5$ Hz, $P_v = 75$ MPa, and $T_m = 230$ °C, the diffraction pattern of the skin layer is the same as that of the static sample, as shown in Fig. 5b. But the diffraction patterns of the core layer and the transition layer are greatly different from those of the static sample, as shown in Fig. 5d, f. It is noted that some Debye rings of those layers exhibit arcing and indicate orientation. Moreover, in the diffraction pattern of the transition layer, the existence of the ring of (300) β indicates β-form crystal exists in the layer.

Using the Hermans orientation function, the orientation level of various planes could be quantitatively evaluated according to

$$f = \frac{3\langle \cos^2 \varphi \rangle - 1}{2} \tag{1}$$

$$\langle \cos^2 \varphi \rangle = \frac{\int_0^{\frac{\pi}{2}} I(\phi) \sin \phi \cos^2 \phi \mathrm{d}\phi}{\int_0^{\frac{\pi}{2}} I(\phi) \sin \phi \mathrm{d}\phi} \tag{2}$$

where φ is the angel between the normal of a given (*hkl*) crystal plane and shear flow direction, and I is the intensity. Its limiting values of orientation parameter f,

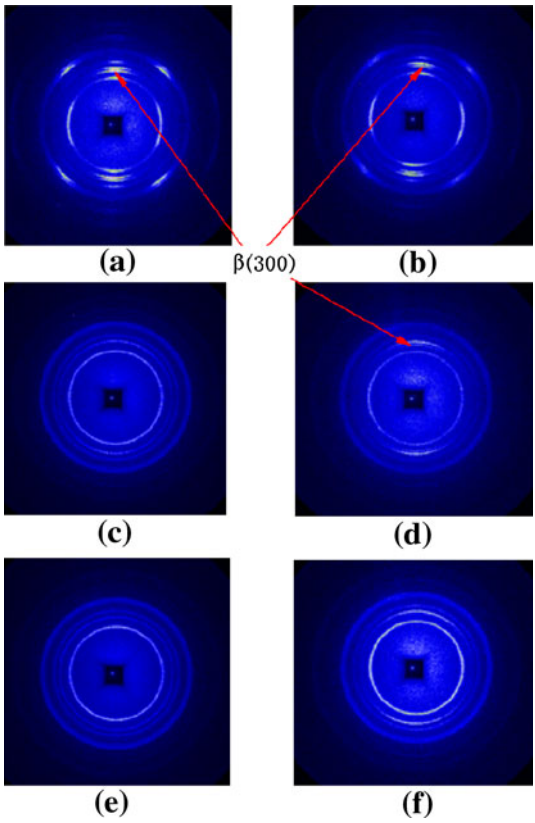

Fig. 5 2D-WAXD pattern of **a** the skin layer of static sample, **b** the skin layer of vibration sample, **c** the transition layer of static sample, **d** the transition layer of vibration sample, **e** the core layer of static sample, and **f** the core layer of vibration sample. The vibration sample was prepared under the processing parameters of $f = 0.5$ Hz, $P_v = 75$ MPa, and $T_m = 230$ °C

taking $\varphi = 0°$ as the shear flow direction, are -0.5 for a perfectly perpendicular orientation and 1.0 for a perfectly parallel orientation. An un-oriented sample gives $f = 0$.

The (040) reflection in this study is chosen to quantitatively evaluate the orientation level of static and vibration sample, and intensities of the reflection is plotted against the azimuth angle from 0° to 360°, in which 0° represents the equatorial (ND) direction, as shown in Fig. 6. The orientation parameters estimated from azimuthal 2D-WAXD pattern of (040) reflection are listed in Table 2. For the core layer and the transition layer of static sample, the orientation parameters tend to zero (0.058), which clearly implies that random orientation is presented in those layers. However, for the vibration samples, the orientation parameters of the core layer and the transition layer are 0.222 and 0.457, which indicates some extents of orientation in those layers. For the skin layers, either the static sample (0.946) or the vibration sample (0.905) has high orientation parameters. It indicates pronounced orientation which is due to the complex combination of high shear stresses imposed on iPP melt and fast cooling rate near the mold surface.

For the static sample, the combination of lower shear stress and cooling rate causes that random orientation is presented in the core layer and the transition layer. But for the vibration sample, a periodical pressure is imposed on the iPP melt during

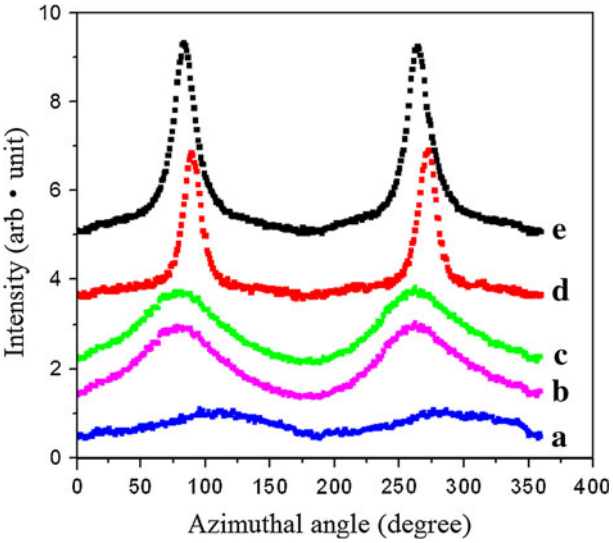

Fig. 6 The azimuthal profiles of (040) reflection of **a** the core layer and transition layer of static sample, **b** the core layer of vibration sample, **c** the transition layer of vibration sample, **d** the skin layer of static sample, and **e** the skin layer of vibration sample. The flow direction is vertical

Table 2 Orientation parameters estimated from azimuthal 2D-WAXD pattern of (040) reflection of layers

	Orientation parameters (f)		
	The skin layer	The transition layer	The core layer
Static sample	0.947	0.058	0.058
Vibration sample	0.905	0.457	0.222

the cooling solidification, so there is always a shear stress exists at the solid-melt interface. With the progress of the solidification, the interface orients layer by layer. Therefore, some extents of orientation can be achieved in the transition and core layers. Because the cross-section of the gate decreases gradually, the shear strength also decreases. So, the orientation of inner layer is lower than that of out layer.

PLM observation

As is well-known, the morphology of injection molding sample is composed of regions called skin, transition, and core region. The skin region is often considered to be thin and essentially characterized by a relatively high amorphous content due to rapid cooling. The lower cooling rate in the core region can allow complete relaxation of the molecule chains and growth of spherulites (monoclinic α-form for iPP [26]) which is almost the same as those grown from the quiescent cases. The transition zone, which is formed under relatively high melt temperature and shear flow, is composed of oriented row structure crystallites (mixed α- and β-form for

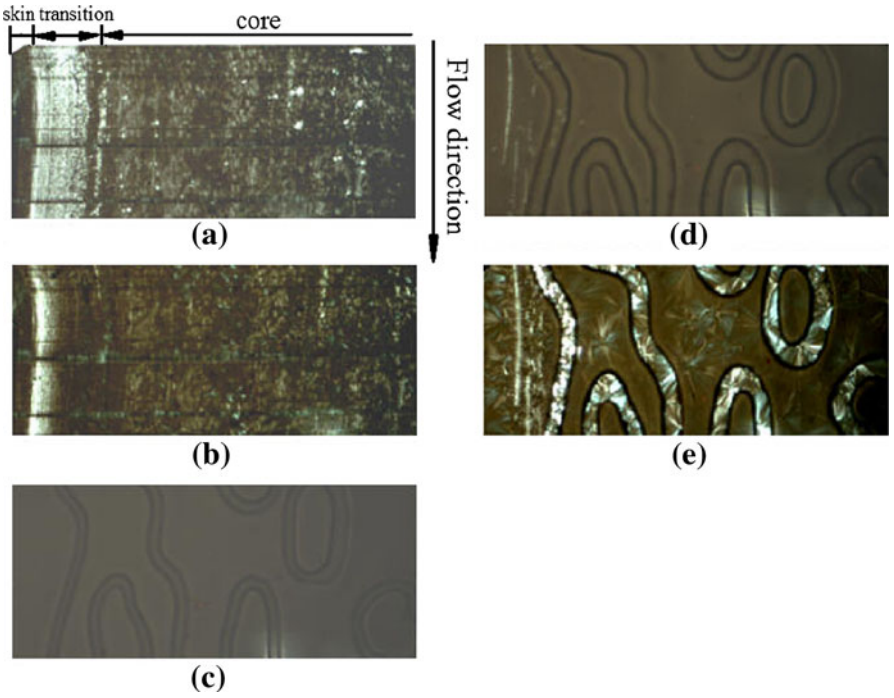

Fig. 7 Optical pictures of vibration injection specimen prepared under the processing parameters of $f = 0.5$ Hz, $P_v = 75$ MPa, and $T_m = 230$ °C: **a** original morphology taken at $T = 25$ °C, **b** heating to $T = 147$ °C, **c** $T = 164$ °C, **d** cooling to $T = 139$ °C after holding at 180 °C for 2 min, and **e** cooling to $T = 25$ °C

iPP [26]). In order to identify the crystal structure of vibration injection specimen, PLM observation was performed.

Skin–core morphology of vibration injection specimen prepared under the processing parameters of $f = 0.5$ Hz, $P_v = 75$ MPa, and $T_m = 230$ °C is shown in Fig. 7a, taken at 25 °C. Slice was cut from the sample at the same depth of 1.5 mm from the surface as that of 1D-WAXD measurement. In the transition region, row structure composed of closely packed fiber crystals orients along the flow direction. Tiny and bright crystallites are densely dispersed in the region near the core, which were proven to be β-PP in the melting process. In the core region, some big and bright crystallites which are also β-PP could be observed. In Fig. 7b, at 147 °C near the melting peak temperature of β-PP, β crystallites in the transition and core region melted while the α-crystals still existed. No change took place until the temperature rose to 158 °C at which α-crystal begun to melt, and then α-crystal became completely invisible at 164 °C, as shown in Fig. 7c. Then, the specimen was isothermally treated at 180 °C for 2 min. Decreasing the temperature down to 139 °C, some fiber crystals reappeared in the transition region before the bulk crystallization as shown in Fig. 7d. This phenomena could be explained by the structure memory effect [33]: fiber crystal is composed of highly oriented molecule

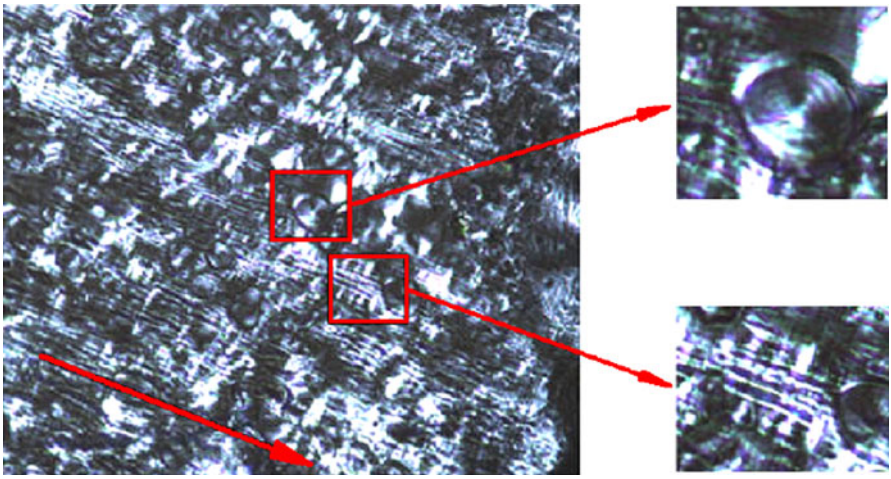

Fig. 8 Optical pictures of core region of vibration injection specimen prepared under the processing parameters of $f = 0.5$ Hz, $P_v = 75$ MPa, and $T_m = 230$ °C, taken at higher magnification. The *arrow* indicates the flow direction

chains induced by shear stress; due to their high thermal stability, the oriented chains could partly preserve their stretching state even after being heated above the melting point of α-iPP, and induce self-nucleation through the formation of row nucleus; these row nucleus begin to crystallize at a higher temperature than the homogeneous or heterogeneous ones. Row nucleus induced an epitaxial growth of crystallites leading to formations of cylindritic structure, as shown in Fig. 7e. Epitaxial crystallization can only grow perpendicular to the row nucleus due to the large aspect ratio until impingement with spherulites.

Padden and Keith [1] divided the spherulite of iPP into five types, two of which are β-form. Under PLM, one type of β-form (β_{III} [34]) is of negative radial birefringence feature and always looks brighter than the other crystallines. The other type of β-form (β_{IV} [34]) is characteristic of its unique negative rings in all types of iPP spherulites. In addition, they crystallize at different temperature: β_{III} below 128 °C and β_{IV} between 128 and 132 °C. Figure 8 shows the core region of vibration injection specimen prepared under the processing parameters of $f = 1.5$ Hz, $P_v = 35$ MPa, and $T_m = 230$ °C. Two types of β crystallines can be observed simultaneously. The bright β-form crystallites are fan-shaped and lie perpendicularly to the flow direction. Meanwhile, the ringed β crystallites almost remain its spherulite shape. The coexistence of the two types of β crystalline has not been observed in the injection molding process as far as we know. Note that, lots of fiber crystallites orient along flow direction, and fan-shaped β crystallites seem to grow from the fiber crystallines, as marked in the Fig. 8. Varga [34] stated that row nucleus can induce cylindrites of α-form at a high temperature above the upper limit crystallization temperature of β-form. At the temperature range of β-form crystallization, however, punctiform β-nuclei may also be formed on a row nucleus of α-form or on the growing cylindritic front through β-α growth transition. Only if

shear load acts on the melt, can the β-α growth transition take place [35]. Then dispersed β-nucleus on the growing cylindritic front grow only in one direction due to the restricting of surrounding α-cylindrites. The existence of β-modification crystallines indicates that vibration injection is able to impose additional shear effect on the specimens even in the core region and influence the crystal structures and morphology.

Conclusion

This study dealt with the effects of vibration field on the crystal structures and orientation of iPP sample. In the process of vibration injection, the imposition of pulsant pressure on the melt can bring about additional shear effect during the injection and packing stages. The major conclusions are summarized as follow:

1. The β-form and γ-form of iPP exist in vibration injection molding sample. Moreover, the orientation of iPP chains within lamellae is observed in the transition layer and the core layer of vibration sample.
2. Skin–core multilayer morphology is observed in the specimen prepared under the processing parameters of $f = 0.5$ Hz, $P_v = 75$ MPa, and $T_m = 230$ °C. In the heating process, β-form crystal is proven to exist in transition and core region.
3. Two types of β-form crystalline can be observed simultaneously in core region. The bright β crystallites (β_{III}) are fan-shaped and lie perpendicularly to the flow direction and the ringed β crystallites (β_{IV}) almost remain their spherulite shape.
4. There is row structure crystalline composed of densely accumulated fiber crystal in the core region. This implies vibration injection can bring about shear effect even in the core. Besides β_{III} crystallites seem to grow from the fiber crystallines.
5. Fiber crystal in the transition region is of high thermal stability, and can reappear in the cooling circle after being heated to 180 °C which is higher than the melting point of α-PP.

Acknowledgments We would like to express our great thanks to National Natural Science Foundation of China (50873072, 50803038), and the Special Funds for State Key Laboratory, for financial support.

References

1. Padden FJ, Keith HD (1959) Spherulitic crystallization in polypropylene. J Appl Phys 30:1479–1484
2. Jones AT, Aizlewood JM, Beckett DR (1964) Crystalline forms of isotactic polypropylene. Makromol Chem 75:134–158
3. Bruckner S, Meille SV, Petraccone V, Pirozzi B (1991) Polymorphism in isotactic polypropylene. Prog Polym Sci 16:361–404
4. Lotz B, Wittmann JC, Lovinger AJ (1996) Structure and morphology of poly(propylenes): a molecular analysis. Polymer 37:4979–4992

5. Fujiwara Y (1975) Das doppelschmelzverhalten derβ-phase des isotaktischen polypropylens. Colloid Polym Sci 253:273–282
6. Leugering HJ, Kirsch G (1973) Beeinflussung der kristallstruktur von isotaktischem polypropylen durch kristallisation aus orientierten schmelzen. Angew Makromol Chem 33:17–23
7. Varga J, Karger-Kocsis J (1996) Rules of supermolecular structure formation in sheared isotactic polypropylene melts. J Polym Sci Pol Phys 34:657–670
8. Varga J, Ehrenstein GW (1996) Formation of stage of crystallization. Polymer 37:5959–5963
9. Varga J (2002) β-modification of isotactic polypropylene: preparation, structure, processing, properties, and application. J Macromol Sci Phys 41:1121–1171
10. Leugering HJ (1967) Einfluß der kristallstruktur und der überstruktur auf einige eigenschaften von polypropylen. Makromol Chem 109:204–216
11. Shi G, Zhang X, Qiu Z (1992) Crystallization kinetics of β-phase polypropylene. Makromol Chem 193:583–591
12. Ikeda N, Kobayashi T, Killough L (1996) Novel β-nucleator for polypropylene; polypropylene '96. World Congress, Zurich, 18–20 Sept 1996
13. Ibar JP (1998) Control of polymer properties by melt vibration technology: a review. Polym Eng Sci 38:1–20
14. Varga J, Mudra I, Ehrenstein GW (1999) Highly active thermally stable β-nucleating agents for isotactic polypropylene. J Appl Polym Sci 74:2357–2368
15. Mathieu C, Thierry A, Wittmann JC, Lotz B (2002) Specificity and versatility of nucleating agents toward isotactic polypropylene crystal phases. J Polym Sci Part B Polym Phys 40:2504–2515
16. Jones AT (1971) Development of the gamma-crystal form in random copolymers of propylene and their analysis by DSC and X-ray methods. Polymer 12:487–508
17. Kardos JL, Christiansen AW, Bear EA (1966) Structure of pressure-crystallized polypropylene. J Polym Sci A 2 Polym Phys 4:777–788
18. Bevis MJ, Kalay G (1997) Processing and physical property relationships in injection-molded isotactic polypropylene. 2. Morphology and crystallinity. J Polym Sci Part B Polym Phys 35:265–291
19. Karger-Kocsis J, Varga J, Ehrenstein GW (1997) Comparison of the fracture and failure behavior of injection-molded α- and β-polypropylene in high-speed three-point bending tests. J Appl Polym Sci 64:2057–2066
20. Karger-Kocsis J, Varga J (1996) Effects of β-α transformation on the static and dynamic tensile behavior of isotactic polypropylene. J Appl Polym Sci 62:291–300
21. Kantz MR, Newman JHD, Stigale FH (1972) The skin-core morphology and structure-property relationships in injection-molded polypropylene. J Appl Polym Sci 16:1249–1260
22. Fujiyama M, Awaya H, Kimura S (1977) Mechanical anisotropy in injection-molded polypropylene. J Appl Polym Sci 21:3291–3309
23. Ibar JP (1995) Improving molding through melt-flow oscillation. Mod Plast 25(85):87–91
24. Guan Q, Shen KZ, Ji LL, Zhu JM (1995) Structure and properties of self-reinforced polyethylene prepared by oscillating packing injection-molding under low-pressure. J Appl Polym Sci 55:1797–1804
25. Guan Q, Shen KZ, Zhu JM (1996) Structure and properties of self-reinforced polypropylene in oscillating stress field. Acta Polym Sin 6:378–381
26. Jiang CD, Shen KZ (1998) Study of preparation of biaxially self-reinforced HDPE samples under unidirectional shearing field of low pressure (I): analysis of aggregation morphology of samples. China Plastics Ind 26:99–102
27. Wang Y, Zhang Q, Fu Q (2003) Compatibilization of immiscible poly(propylene)/polystyrene blends using clay. Macromol Rapid Comm 24:231–235
28. Na B, Zhang Q, Fu Q, Zhang G, Shen KZ (2002) Super polyolefin blends achieved via dynamic packing injection molding: the morphology and mechanical properties of HDPE/EVA blends. Polymer 43:7367–7376
29. Kalay G, Allan P, Bevis MJ (1995) Microstructure and physical property control of injection moulded polypropylene. Plast Rubb Proc Appl 23:71–85
30. Kalay G, Bevis MJ (1997) Processing and physical property relationships in injection molded isotactic polypropylene. 1. Mechanical properties. J Polym Sci Pol Phys 35:241–263
31. Zhang J, Shen K, Na S, Fu Q (2004) Vibration-induced change of crystal structure in isotactic polypropylene and its improved mechanical properties. J Polym Sci Pol Phys 42:2385–2390
32. Zhang J, Zeng T, Zhu J, Lei YW, Shen KZ, Fu Q (2007) Crystal form and orientation of isotactic polypropylene samples prepared by vibration-injection molding. J Appl Polym Sci 106:1456–1461

33. Varga J (1983) Characteristics of cylindritic crystallization of polypropylene. Angew Makromol Chem 112:191–203
34. Varga J (1992) Supermolecular structure of isotactic polypropylene. J Mater Sci 27:2557–2579
35. Varga J, Karger-Kocsis J (1993) Direct evidence of row-nucleated cylindritic crystallization in glass fiber-reinforced polypropylene composites. Polym Bull 30:105–110